Available online at www.sciencedirect.com
ScienceDirect
Cement & Concrete Composites 29 (2007) 230–240
Cement & Concrete Composites
www.elsevier.com/locate/cemconcomp

Effect of specimen size on flexural compressive strength of reinforced concrete members

Seong-Tae Yi [a,*], Min-Su Kim [b], Jin-Keun Kim [b], Jang-Ho Jay Kim [c]

[a] Department of Civil Engineering, Chung Cheong University, 330, Wolgok-ri, Kangnae-myun, Cheongwon-kun, Chungbuk-do 363-792, South Korea
[b] Department of Civil & Environmental Engineering, Korea Advanced Institute of Science and Technology, 373-1, Kuseong-dong, Yusong-gu, Daejeon-si 305-701, South Korea
[c] Department of Civil & Environmental Engineering, Yonsei University, 134 Shinchon-dong, Seodaemun-gu, Seoul-si, 120-749, South Korea

Received 11 July 2006; received in revised form 6 November 2006; accepted 11 November 2006
Available online 11 January 2007

Abstract

It is important to consider the effect of member size when estimating the ultimate strength of a concrete flexural member, because the strength always decreases with an increase of member size except for well-reinforced members. Research conducted previously in this area include axial compressive strength size effect on cylindrical specimens and flexural compressive strength size effect on C-shaped specimens, notched cylindrical specimens, and axially loaded double cantilever beam (DCB) specimens. Since the most widely used flexural member type is reinforced concrete (RC) beams, it is logical to extend the study of flexural compressive strength size effect to flexural loaded RC beam members. Previously, several researchers have reported from their studies that flexural compressive strength size effect does not exist. However, the analyses show that the specimens used for the study had limited size variation and the neutral axis depth variations were too similar to show distinct size effect. Therefore, this study enforced distinct neutral axis depth variations for all of the tested specimens.

In this study, the size effect of a RC beam was experimentally investigated. For this purpose, a series of beam specimens subjected to four-point loading was tested. RC beams with three different effective depths were tested to investigate the size effect. The shear-span to depth ratio and the thickness of the specimens were kept constant to eliminate the out-of-plane size effect.

The test results are curve fitted using Levenberg–Marquardt's Least Square Method (LSM) to obtain parameters for Modified Size Effect Law (MSEL) by Kim et al. The analysis results show that the flexural compression strength and ultimate strain decrease as the specimen size increases. Comparisons with existing research results considering the depth of neutral axis were also performed. They also show that the current strength criteria-based design practice should be reviewed to include member size effect.

Keywords: Size effect; Flexural member; Flexural compressive strength; Stress–strain relationship; Modified size effect law (MSEL)

1. Introduction

Currently, researchers in the field of fracture mechanics of concrete structures accept the conclusion that the failure of concrete loaded in tension is caused by strain localization that results in a finite size fracture process zone. In the last few years, many researchers [1,2] have begun to realize that strain localization also occurs for concrete specimens loaded in compression; however, the compressive failure mechanism is more complex than the tensile failure mechanism. In addition, the formation of micro-cracks in compressive failure is distributed in a wider region than in tensile failure.

For the compression-loaded concrete specimens, there are no observable cracks unlike tension-loaded specimen. This is because concrete has nearly ten fold greater strength

* Corresponding author. Tel.: +82 43 230 2315; fax: +82 43 230 2319.
E-mail address: yist@ok.ac.kr (S.-T. Yi).

0958-9465/$ - see front matter © 2006 Elsevier Ltd. All rights reserved.
doi:10.1016/j.cemconcomp.2006.11.005

Nomenclature

a	shear-span length	l_0	width of crack band ($=\lambda_0 d_a$)
A_1, A_2, A_3, A_4	coefficients of cubic equation $f_c = A_1 + A_2\varepsilon_c + A_3\varepsilon_c^2 + A_4\varepsilon_c^3$	M	bending moment in the central cross-section
		P_u	maximum load, or ultimate axial load
b	thickness of specimen	R^2	correlation coefficient
B, α	empirical constants	s	standard deviation
c	depth to neutral axis of critical section of beam specimen or C-shaped specimen	α_1	width of equivalent rectangular stress block
		β_1	depth of equivalent rectangular stress block
D	characteristic dimension	ε_c	strain in concrete
d	effective depth, distance from compression face to centroid of tensile steel	ε_u	ultimate strain in concrete
		κ	curvature
d_a	maximum aggregate size	λ_0	approximate constant (=2.0)
E_c	elastic modulus of concrete	ρ	radius of curvature
f_c	stress in concrete	σ_0	size-independent stress ($=\alpha f_t'$)
f_c'	uniaxial compressive strength of standard concrete cylinder	σ_N	nominal flexural compressive strength at failure in beam
f_{ct}	splitting tensile strength of concrete cylinder	ρ_t	tensile reinforcement ratio
f_t'	direct tensile strength	υ	deflection

in compression than in tension. However, stress is definitely concentrated at the crack tip region and micro-cracks form in the loaded direction [3,4]. As the load increases, one or several macro-cracks are formed by the coalescence of these micro-cracks ultimately leading to a failure. Occurrence and development of micro-cracks and the typical pattern of compressive failure are described in detail in a research performed by Bazant and Xiang [5]. This phenomenon is more apparent as the specimen size increases.

Based on the stress concentration rate due to the loading type or specimen configuration, the intensity of size effect is determined. More specifically, a rate of stress concentration at the front of crack tips for a member loaded in compression is significantly slower than a member loaded in tension. Therefore, tensile member has more remarkable size effect than compressive member. In a tensile loaded member, the stress applied at the crack tip region is pure tensile stress. On the other hand, a member loaded in compression applies a combination of tensile and compressive stresses at the crack tip region. Since tensile stress most rapidly brings about stress concentration at the crack tip region, the size effect of tension specimens is much more distinct than in compression specimens. At present, most design codes for concrete structures do not consider the effect of size.

Concrete is a construction material normally used to withstand compressive force. Even though the failure mechanism of tensile failure is different than that of compressive failure, the ultimate failure in both specimens is due to the propagation of macro-cracks that indicate localized tension or Mode I failures followed by mixed-mode behavior, such as in compressive failures or shear failures. Therefore, it is safe to assume that the tensile fracture-based concept can be applied to compressive failure as well. For this reason, several researchers are currently performing a number of studies regarding the compressive failure of concrete. In past studies, Gonnerman [6] experimentally showed that the ratio of the compressive failure stress to the compressive strength decreases as the specimen size increases. Markeset and Hillerborg [7] and Jansen and Shah [8] also experimentally showed that strength reduction is independent of the specimen size when the specimen height/diameter is greater than a constant value (i.e., 2.0–2.5 for cylindrical specimens). Currently, Fantilli et al. [9] have studied the size effects on beam ductility caused by the depth of the compression zone. Moreover, based on the previous concept, the fracture mechanics-type size effect for diagonal shear failure of beams [10] and empirical modeling of reinforced concrete (RC) shear strength size effect for members [11] were carried out to verify failures in concrete structures.

The actual stress distribution in the compression zone of RC flexural members is extremely difficult to both measure and adequately model. In 1955, Hognestad et al. [12] experimentally presented a concrete stress distribution in an ultimate strength design via a rising curve from zero to maximum stress, and a descending curve beyond the maximum stress. The test procedure on C-shaped concrete specimens subjected to axial load and bending moment was developed by the Portland Cement Association (PCA) [12,13] and at the time formed the basis of the rectangular stress block used in the ACI 318 Code [14]. In addition, the findings of Kim et al. [15–17] have shown that under flexural compression loading the failure strengths decrease as the sizes (that is, size, length, and depth variations) of the concrete specimens increase. Given that the most widely used flexural member type is an RC beam, it is logical to extend the study of the flexural compressive strength size effect to flexural loaded RC beam members. At present, however, both experimental and analytical

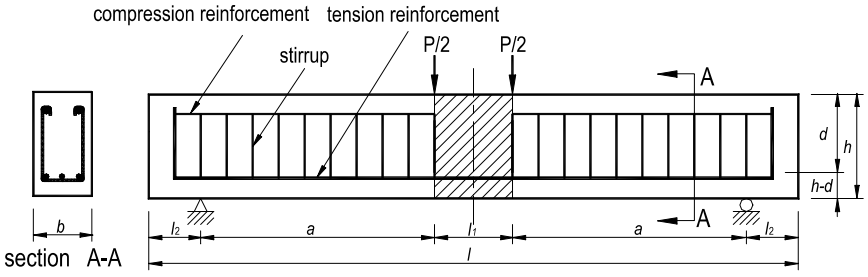

Fig. 1. Shape and dimensions of specimens.

studies concerning the depth of the neutral axis for RC beam specimens are scarce due to the numerous difficulties encountered in measuring the stress–strain distribution experimentally.

The purpose of the present study is to experimentally investigate the size dependency on flexural compressive strength, more specifically the flexural strength of RC beams, considering the depth of the neutral axis. Previously, several researchers [18] have reported from their studies that a size effect for the flexural compressive strength does not exist. However, the analyses show that the specimens used for the study had limited size variation and the neutral axis depth variations were too similar to show a distinct size effect. Therefore, this study enforced distinct neutral axis depth variations for all of the tested specimens. Furthermore, analytical equations that reasonably predict the size effect of flexural compressive strength are proposed based on experimental data obtained from flexural tests of RC beam specimens, which is designed and constructed in the actual field.

2. Application of MSEL to failures in concrete

After deriving size effect law (SEL) by Bazant [19], Kim et al. [20] proposed the MSEL (Eq. (1)) by adding the size-independent strength $\sigma_0(=\alpha f_t')$ to SEL that can predict the strength of concrete members with or without initial cracks and with similar or dissimilar cracks. This concept is also proposed by Bazant and Xiang [5] and Bazant [21,22] with a different approach.

$$\sigma_N = \frac{Bf_c'}{\sqrt{1+\frac{D}{\lambda_0 d_a}}} + \alpha f_c' \quad (1)$$

where σ_N is the nominal strength, f_c' is the compressive strength of standard cylinder, D is the characteristic dimension, d_a is the maximum aggregate size and B, λ_0, and α are empirical constants.

As an application of MSEL, some researches [15–17,23,24] have been performed on unnotched and notched cylindrical specimens subjected to uniaxial compressive force, axially loaded Double Cantilever Beam, and C-shaped specimens subjected to flexural compression force. Meanwhile, Yi et al. [25] reported the research results on the effect of specimen sizes, specimen shapes, and placement directions on compressive strength of concrete. In Eq. (1), the width of crack band l_0 is empirically found to be related to the maximum aggregate size, e.g., $l_0 = \lambda_0 d_a$ in which λ_0 is an approximate constant with values between of 2.0 and 3.0 [15,16,23]. In the regression analysis, this constant is selected as 2.0 where $l_0 = 2.0 \times d_a = 4.0$ cm.

3. Test specimens and experimental program

3.1. Test specimens

The dimensions, shape, loading point locations, specimen number, and reinforcement details of specimens used in the experiments are shown in Fig. 1 and Table 1. The main test variable was effective depth of the specimen ($d = 15$, 30, and 60 cm), with the same concrete compressive strength of 37 MPa. The shear-span to depth ratio ($a/d = 3.0$) and the thickness ($b = 20$ cm) was kept constant so that the effect of thickness of specimen on the size effect can be eliminated. The central section of beam, the critical section under flexural compression loading, was not reinforced with shear reinforcement. The reinforcement, as shown in Fig. 1, was used at the two ends of the specimen to eliminate the shear failure at the two end sections.

According to Table 1, tensile reinforcement ratios are different for different specimen sizes. The difference is to consider slight variations of yield strengths for various reinforcing bar diameters as shown in Table 2. In this experiment, tensile reinforcement ratios were adjusted to

Table 1
Specimen size type and reinforcement details

Specimen no.	I	II	III
h (cm)	65	35	20
d (cm)	60	30	15
l_1 (cm)	60	30	15
l (cm)	460	230	125
a (cm)	180	90	45
l_2 (cm)	20	20	20
Tensile reinforcement	2-D25 + D19	2-D16 + D19	3-D13
Compressive reinforcement	2-D10	2-D10	2-D10
Stirrup	D10@200	D8@100	D6@50
Tensile reinforcement ratio (ρ_t) (%)	1.11	1.14	1.33
ρ_t/balanced reinforcement ratio	0.45	0.44	0.42

Table 2
Reinforcing bar strengths

	Yield strength, f_y (MPa)	Ultimate strength, f_u (MPa)	f_u/f_y
D13	390.83	582.32	1.49
D16	445.28	666.30	1.50
D19	473.23	693.27	1.46
D25	467.55	697.10	1.49

represent the same failure behavior for all specimens at the time of yielding of reinforcing bars.

The concrete mixture proportions and physical properties selected for the beam and 28-day compressive strength cylinder specimens are given in Table 3 where w, c, s, and g represent the unit weights of water, cement, sand, and gravel, respectively. The design strength and slump are 35 MPa and 12 cm, respectively. Type I Portland cement was used in all mixtures. Crushed gravel is used as the coarse aggregate and the maximum aggregate size d_a is 20 mm. As listed in Table 3, concrete compressive strength f'_c, splitting tensile strength f_{ct}, and elastic modulus E_c are averaged values from testing of three identical $\varnothing$ 100×200 mm cylinders in the series. Specimens are cast vertically on a level surface. Two specimens per specimen size, totally six specimens, are prepared. All beam specimens and cylinders were removed from the mold after 24 h and dry-cured under a wet burlap/tower until testing. The cylinders were tested at an age similar to the concrete used for the beam specimens.

The numbering of the specimen (that is, I-1) and experimental data are tabulated in Table 5. Also, the roman numerals I–III represent the size of the specimens with I being the largest and decreasing accordingly. The arabic numbers 1 and 2 are the two specimens tested for each specimen size.

3.2. Experimental program

The applied loads in four-point loading shown in Fig. 1 was supplied by a universal testing machine (UTM) with a capacity of 2500 kN using a displacement control method. During testing, loads were measured up to failure by load cells. The horizontal thick solid lines in Fig. 2 represent the locations where strain gages are attached to the sides of specimens. As shown in Fig. 2 and Table 4, strains were measured using strain gages attached to each side of the plane of symmetry of the specimens I–III, correspondingly. The strain gages in the compression zone were attached more closely than the tension zone. In addition, 8, 6, and 6 linear variable displacement transducers (LVDTs) were used to monitor vertical displacements at each side of specimens I–III, correspondingly.

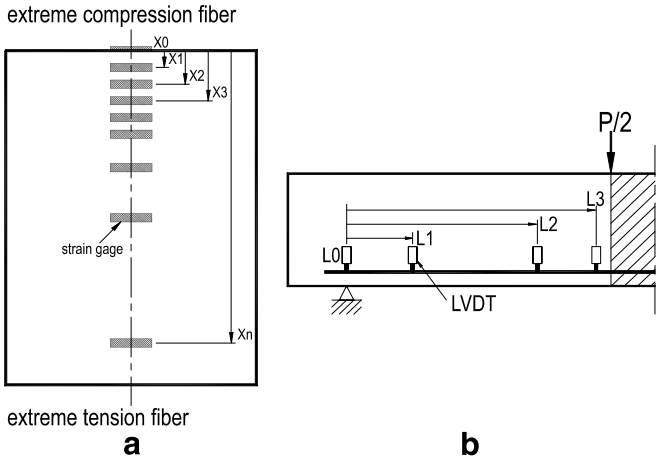

Fig. 2. Locations of strain gages and LVDTs: (a) strain gages and (b) LVDTs.

Table 4
Locations of strain gages and LVDTs

Specimen size type	X_i[a] for strain gage (cm)	L_i[a] for LVDT (cm)
I	0, 2, 4, 6, 8, 10, 14, 20, 30, 40, 60	0, 37, 115, 165, 255, 305, 383, 420
II	0, 1, 2, 3, 4, 5, 7, 10, 15, 20, 30	0, 35, 85, 125, 175, 210
III	0, 1, 2, 3, 4, 5, 7, 10, 15	0, 11, 39, 66, 94, 105

[a] Length measurements indicated in Fig. 2.

4. Experimental results and evaluation

4.1. Test results

In Table 5, σ_N, P_u, $\varepsilon_{u,test}$, and $\varepsilon_{u,anal}$ represent the nominal flexural compressive strength, maximum load, ultimate strain obtained from experiments at failure, and the ultimate strain obtained from analyses at failure, correspondingly. In Eq. (1), the strength in concrete σ_N is the maximum stress value in the stress–strain curve. All specimens were tested successfully where stable failure occurred in the middle section of specimens as shown in Fig. 3. $\varepsilon_{u,test}$ is neither ultimate strain value nor the corresponding strain value at the maximum stress, but it is a reasonable maximum strain value measured using the strain gages located in the extreme compression fiber. The reason for using this

Table 3
Concrete mixture proportions and physical properties of concrete

w/c (%)	$s/(s+g)$ (%)	Unit weight				f'_c(MPa)	f_{ct} (MPa)	E_c (MPa)
		w (kg/m^3)	c (kg/m^3)	s (kg/m^3)	g (kg/m^3)			
45	39	186	409	643	1017	37	4	27,700

Table 5
Test results of beam specimens

Specimen no.	σ_N (MPa)	P_u (kN)	$\varepsilon_{u,test}$ ($\times 10^{-6}$)	$\varepsilon_{u,anal}$ ($\times 10^{-6}$)
I-1	37.57	486.58	2200	2825
I-2	36.10	479.71	2270	2720
II-1	39.73	247.21	3080	3245
II-2	40.42	243.29	2990	3130
III-1	43.46	128.51	3370	4110
III-2	42.67	126.55	3410	4420

strain value is due to the fact that an accurate strain cannot be obtained in the descending branch of stress–strain relationship when the failure starts in the fiber of concrete beams (i.e., beyond the maximum stress). In addition, $\varepsilon_{u,anal}$ is the strain value obtained analytically when the cross-section has a maximum bending moment value in the stress–strain relationship.

During testing, cracks in the central section (i.e., a region without shear reinforcements) for all specimens occurred after formation of diagonal tensile cracks in the parts located between supports and loading points. Finally, as shown in Fig. 3, the failure occurred in the extreme compression fiber of central section with crushing preceding the failure. During testing, concrete showed more brittle failure mechanism as the specimen size increased. This is related to quasibrittle characteristics of concrete materials, energy release rate accumulated in the experimental device, and stiffness of the testing device.

Fig. 4 shows crack patterns at failure. From Fig. 4, it can be seen that more numerous cracks occur as the specimen size increases. However, the relative number of cracks increases with a decreasing specimen size. For the small-size specimen, since the formation of micro-cracks is evenly distributed in a comparatively wide region, it can be noted that size effect is not apparent.

The concrete local to the load application points is under quite different stress conditions than would result from pure flexure. The concrete directly beneath the load points is more highly confined and there will be a diagonal tension field in that region as well. These effects can be seen in the crack patterns and compressive spall zones in Fig. 4. It is generally thought that the disturbed region about statical discontinuities, such as load application points, extends a distance of about one member depth from the source of discontinuity. Other tests on size effect of flexural members provided a relatively larger distance between the load

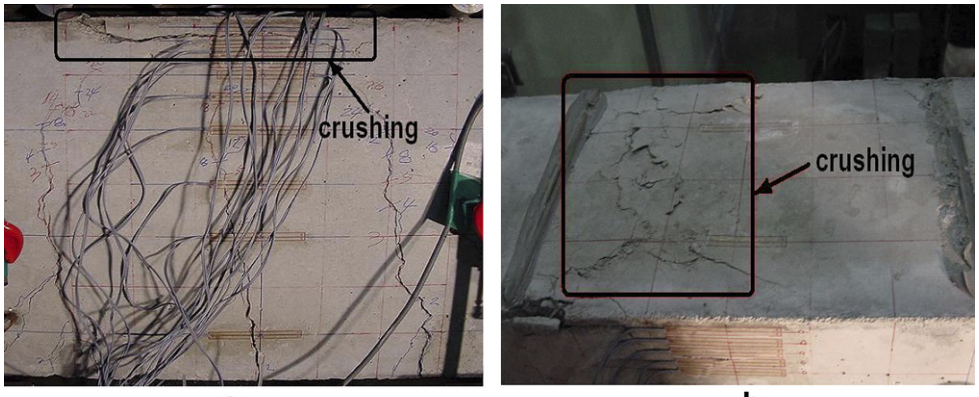

Fig. 3. Crack patterns of specimen II-2 after testing: (a) side surface; and (b) top surface.

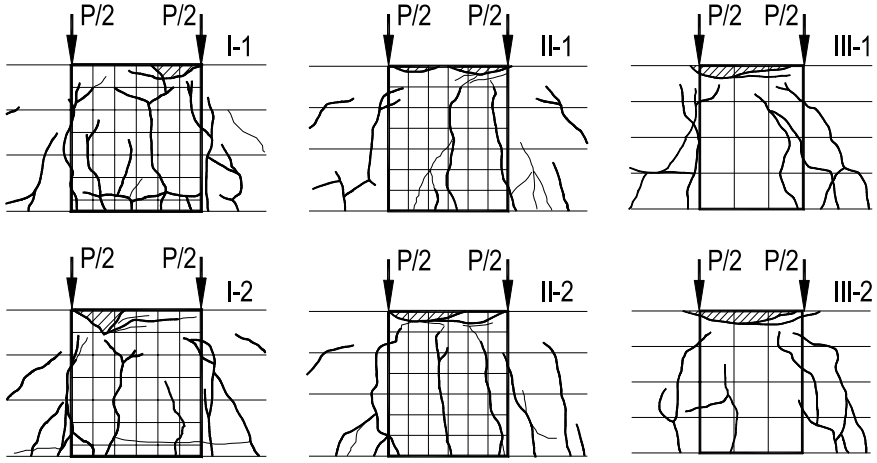

Fig. 4. Typical crack patterns at failure.

points. And, it is also noted that the points of load application disturb the local stress fields and that Bernoulli beam theory does not strictly apply in that central region. In that respect, there are some advantages to the C-shaped specimens.

4.2. Size effect of flexural compressive strength

Fig. 5 shows the normalized normal-strength value $\sigma_N(d)/f'_c$ as a function of the effective depth d, the distance from the extreme compression fiber to the centroid of the steel section. In order to obtain an analytical equation, which predicts the flexural compressive strength of specimens, SEL and MSEL are used. Then, Least Square Method (LSM) regression analyses ([26]; IMSL Library [27]) are performed on the results of the six tested specimens in this study. Cases (1) and (2) of Table 6 are obtained from the analyses and the results are graphed and shown in Fig. 5. Cases (1)–(8) are shown in Table 6. In this figure, the correlation coefficient (R^2) and standard deviation (s) for MSEL are 0.978 and 0.017 and for SEL are 0.975 and 0.018, respectively. In Cases (1) and (2), nominal flexural compressive strength σ_N and uniaxial compressive strength f'_c are in MPa and effective depth of the specimen d is in cm.

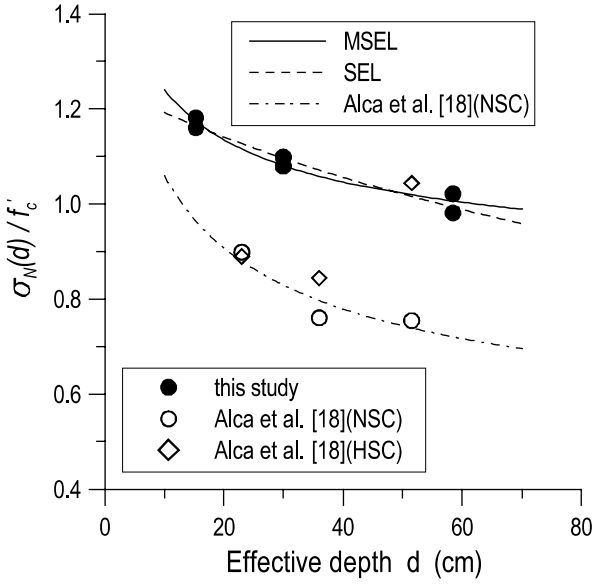

Fig. 5. Relationship between normalized nominal strength and effective depth d.

In this study, we also concluded that the strength ratio approaches a limit with an increasing effective depth d. In Fig. 5, the solid circular data points represent experimental data of this study. In addition, the thick solid line and the dashed line represent the results from Cases (1) and (2), respectively.

As shown in Fig. 5, the results indicate a strong size effect condition. By comparing Cases (1) and (2), it can be seen that the difference is not apparent in the region which contains most of the beam sizes. But, beyond this region, more specifically larger specimen sizes, the new equation (Case (1)) better agrees with the experimental results. Also, MSEL predicts the behavior of specimens having no initial crack or notch more appropriately. If specimens have initial cracks, however, Case (2) is better than Case (1), because the strength decreases continuously as the specimen size increases.

In Fig. 5, the hollow circular data points and the diamond-shape data points represent experimental data of normal-strength concrete (NSC) and high strength-concrete (HSC), respectively, from the reports by Alca et al. [18]. Alca et al. [18] and Corley [28] rejected the hypothesis that there is a size effect in flexure based on the experimental results. From this figure, however, the authors acknowledged that there is a significant evidence of existence of size effect in flexural member, which is supported by the results from this study. In this figure, the one dotted line represents the results from Case (3) for NSC. From the few available experimental data, it is also apparent that the flexural strength decreases as specimen size increases.

4.3. Comparison of proposed and existing model equations based on depth of neutral axis

Fig. 6 shows the normalized normal-strength value as a function of the neutral axis depth c, the distance from the extreme compression fiber to the neutral axis. Cases (4) and (5) are also obtained from the LSM regression analyses on the test data for neutral axis depth. Fig. 6 is a graph of the results obtained from this study. In Cases (4) and (5), depth to neutral axis of beam specimen c is in cm.

Table 6
Parameter values of SEL and MSEL for use in Eq. (1)

Case	B	α	$\lambda_0 d_a$	Usage of c or d	Data source
(1)	0.83	0.79	4.0	d	This study
(2)	1.25	0.00	100.0	d	This study
(3)	1.20	0.42	4.0	d	Alca et al. [18]
(4)	0.60	0.72	4.0	c	This study
(5)	1.23	0.00	25.0	c	This study
(6)	0.71	0.75	2.6	c	Kim et al. [15]
(7)	0.66	0.71	4.0	c	This study and Kim et al. [15]
(8)	0.70	0.47	2.6	c	Kim et al. [15]

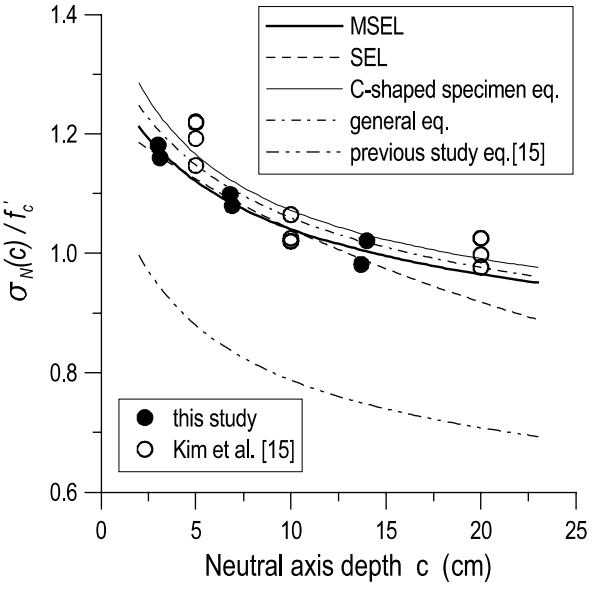

Fig. 6. Relationship between normalized nominal strength and depth to neutral axis c.

Cases (6) and (7) are obtained from the LSM regression analyses on the test data obtained from Kim et al.'s study [15] and a combination of Kim et al.'s study [15] and this study, respectively. Namely, Case (7) is a more general equation since it is derived using all of available data. The results are also graphically shown in Fig. 6. In Case (6) and (7), c is depth of neutral axis of beam specimen or C-shaped specimen in cm. In Kim et al.'s study [15], the maximum aggregate size was 13 mm. Thus, $l_0 = 2.0 \times d_a = 2.60$ cm was used.

In the previous study [15], Case (8) was proposed to obtain the flexural compressive strength of C-shaped specimens with length-depth ratio of 2:1. In Case (8), depth of C-shaped specimen c is in cm.

In this figure, the solid circular data points and the hollow circular data points represent experimental data of this study and Kim et al. [15], respectively. In addition, the thick solid line, the dashed line, the dotted line, the one dotted line, and the two dotted line represent the results from Cases (4)–(8), respectively.

As shown in Fig. 6, the results indicate a strong size effect condition. The comparison of Cases (4)–(7) show that the shape and trend is similar even though a slight scattering between curves smaller and larger specimens exist. However, the $\sigma_N(c)/f'_c$ value of beam specimens is smaller than the value of C-shaped specimens. Thus, an additional value must be considered to accurately obtain beam strength capacity. This difference is probably due to the method obtaining the location of neutral axis, the maximum aggregate size d_a used to obtain the experimental data, and the type of size effect law used (either SEL or MSEL). In addition, the difference between Case (8) and others is due to the fact that the $\sigma_N(c)$ value in Case (8) is calculated as P_u/bc. However, in other cases, $\sigma_N(c)$ means a maximum stress value in the stress–strain curve. It is also important to note that, in order to incorporate the real loading condition, the additional bending moment due to eccentricity should be considered in Case (8).

4.4. Other observations

4.4.1. Location of neutral axis

Fig. 7(a) shows the value of neutral axis location to effective depth ratio as a function of the normalized strain. In this figure, it is important to note that the location of neutral axis with an increasing strain goes up to extreme compression fiber for all size specimens. Also, even though the difference with specimen size is not apparent, the neutral axis is located slightly higher in smaller-size specimens when strain is greater than 0.002. This means that the flexural compressive strength at failure increases as the specimen size decreases.

Fig. 7(b) indicates that the location of neutral axis abruptly changes when the specimens are applied with extreme compression fiber strain of 0.0012–0.0015. This phenomenon, as shown in Fig. 8, occurs on the specimens that lie in the strain range of perfect plastic behavior after tensile reinforcement yielding. This is because the flexural compressive strength increases as the strain increases even though the increase in tensile force is scarce. Accordingly, it is found that the location of neutral axis abruptly rises to satisfy the equilibrium condition between compressive and tensile forces.

4.4.2. Stress–strain relationship

To obtain the stress–strain curve, the extreme compression fiber strain and the location of neutral axis must be compatible. However, when the specimens reach $\varepsilon_{u,test}$ it is difficult to measure strain and neutral axis location. Therefore, the strain shall be obtained from the curvature calculated using moment–displacement relationship. At this time, linear elastic mechanics theory cannot be used, because the deflection of beam is very large. Therefore, the following curvature equation was used.

$$\kappa = \frac{1}{\rho} = \frac{\upsilon''}{[1 + (\upsilon')^2]^{3/2}} \tag{2}$$

where υ is the deflection of the beam when compared to its initial position. For deflections, a cubic equation $f_c = A_1 + A_2\varepsilon_c + A_3\varepsilon_c^2 + A_4\varepsilon_c^3$ data fitted with LSM regression analyses using deflections measured from LVDT's shown in Fig. 2(b) was used.

The experimentally obtained neutral axis location with respect to strain shown in Fig. 7(b) does not nearly change when strain reaches $\varepsilon_{u,test}$. The stress–strain relationship calculated using a cubic equation was obtained by incrementally changing neutral axis depth. The final stress–strain relationship was calculated until the experimentally obtained stress–strain curve of the strain equal to $\varepsilon_{u,test}$ where the neutral axis location no longer changes. When comparing the calculated and experimentally obtained

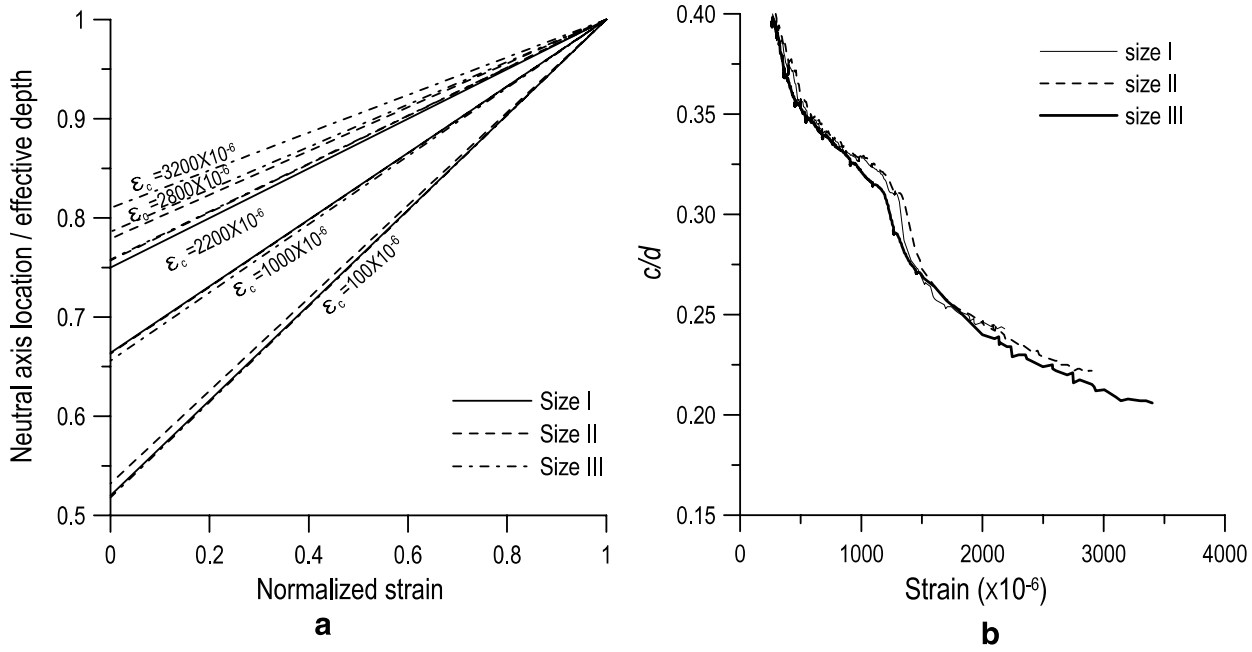

Fig. 7. Variations of neutral axis location with strain in the extreme compression fiber.

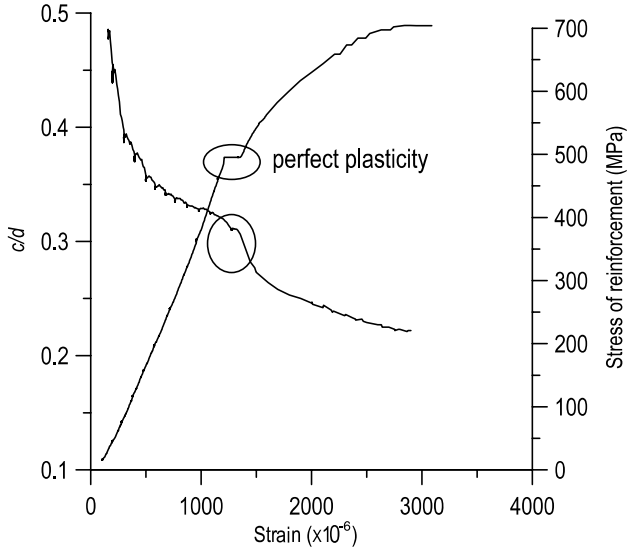

Fig. 8. Variations of neutral axis location due to perfect plasticity of reinforcement with strain.

stress–strain relationships, the difference was not apparent in the ascending branch and an insignificant difference was found in the descending branch. Therefore, it is safe to conclude that in all strain states the calculated stress–strain relationship is valid and similar to the actual beam stress–strain relationship.

The depth of neutral axis has direct relationship to extreme fiber strain of flexural loaded beam members. Stress values on compressed face of specimens f_c obtained from LSM regression analyses using a cubic equation are plotted with respect to strain values on the compressed face ε_c in Fig. 9. LSM regression analysis was performed on the experimental data by satisfying moment equilibrium around the neutral axis of the cross-section. In other words, in order to perform LSM regression, the values of bending moment M and the extreme compression fiber strain ε_c at every loading step are required. Averaged values from two stress–strain curves are plotted with respect to specimen size in Fig. 10. This figure shows generally expected stress–strain relationship.

The thick solid line in Fig. 9 is the uniaxial compressive stress–strain curve obtained from standard concrete cylinder tests. Maximum stress value and the corresponding strain value and the ultimate strain value of beam specimens show a significant increase as the specimen size decreases. The maximum stress value and the corresponding strain value of specimen size III is largest when compared to the other specimen sizes. The stress–strain curves from pure compression of cylindrical specimens and flexure-compression tests of RC beam specimens are similar until the maximum compressive strength f'_c is reached. However, the relationship is significantly different after the peak load. This means that the maximum stress value and the corresponding strain value of beam specimen increases and more ductile behavior occurs as the specimen size decreases.

It is assumed that the established f_c and ε_c relationship is valid for all layers in the cross-section. Thus, a compressive stress can be determined from this relationship using the measured strain value.

4.4.3. Ultimate strain

Fig. 11 is the plot of ultimate strain versus effective depth. It is generally acknowledged that the ultimate strain

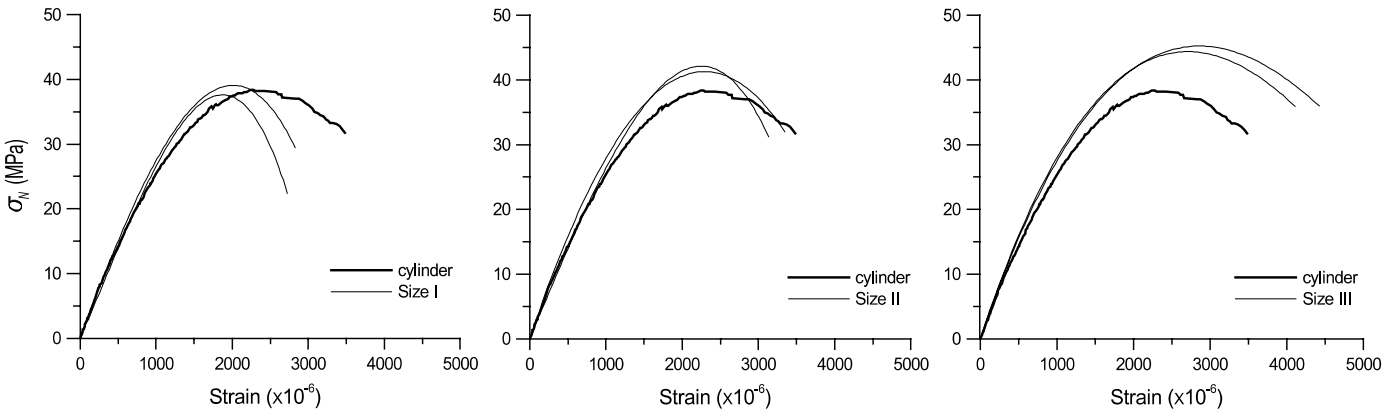

Fig. 9. Comparisons of stress–strain relationship.

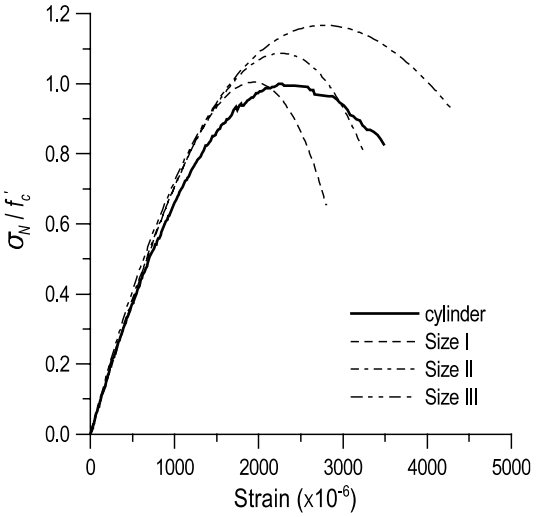

Fig. 10. Effect of specimen size on stress–strain curves.

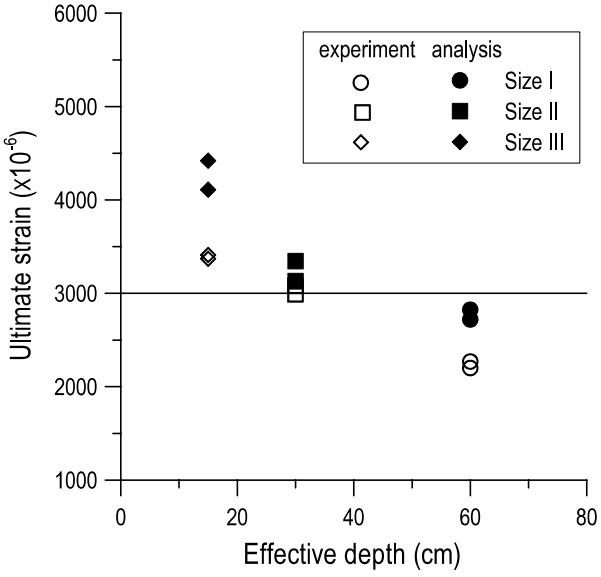

Fig. 11. Relationship between ultimate strain and effective depth.

of concrete ranges between 0.003 and 0.004 [29], based on many experimental results from beams with rectangular cross-section subjected to flexural compression loading. In Fig. 11, the solid line represents the ultimate strain of 0.003 suggested by ACI 318 Code [14]. The test results show that the ultimate strain value of specimen Size I is 0.0028. It is different from the research results reported by Hognestad et al. [12], Kaar et al. [13], Corley [28], and Nedderman [30], and smaller than the value of 0.003. In addition, the strains of specimen Sizes II and III are 0.0032 and 0.00425, respectively, and greater than the constant value. Therefore, in the future study, a more detailed analysis on these values for specimens having bigger specimen sizes should be performed.

This clear size effect trend is probably due to the member size and shape difference as well as to the relative difference of the aggregate size with respect to the specimen size used to obtain the experimental data. More specifically, in the studies performed by PCA and ACI, specimen type was different from this study, (i.e., C-shaped specimens).

4.4.4. Ratio of average compressive stress to maximum stress β_1 based on α_1 value of 0.85

Fig. 12 shows the relationship between ratio of average compressive stress to maximum stress β_1 and specimen effective depth. In Fig. 12, the horizontal solid line represents the β_1 value based on a α_1 value of 0.85. The β_1 value is based on the calculation methodology to obtain a β_1 value following the method suggested by the ACI 318 Code. The ACI approach of using an equivalent rectangular stress block width of $0.85f'_c$ for concrete compressive strength of 37 MPa gives constant β_1 value of 0.78. However, the results show that β_1 values decrease as specimen effective depths increase. In addition, the calculated values are still higher than the test values based on a α_1 value of 0.85. Nilson and Slate [31] also describe β_1 values suggested by the ACI 318 Code is still conservative. Therefore, a more detailed analysis of calculating β_1 values should be performed.

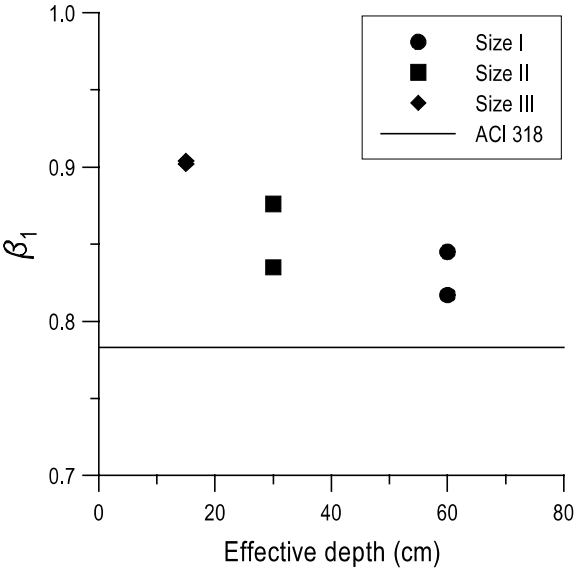

Fig. 12. Relationship between β_1 and effective depth.

5. Conclusions

In order to evaluate the size effect on the flexural compressive strength of RC flexural members considering the depth of neutral axis, a series of flexural tests for six concrete beam specimens and cylinders were carried out. These were cast from the same batch with a compressive strength of 37 MPa. From the test results and analyses, the following conclusions are drawn:

1. Size effect is apparent where the flexural compressive strength at failure and the corresponding strain value and the ultimate strain decrease as the specimen size increases. And, when the specimen size is considerably large, the strain was smaller than the value suggested by the ACI Code suggested value of 0.003. The size effect is also apparent for the stress–strain relationship.
2. New parameter values of MSEL are suggested to better predict the reduction phenomena of the strength.
3. The results show that β_1 values decrease as specimen sizes increase. However, the calculated values are still higher than the constant value assumed in the ACI method.

6. The scope of the work and further experiment

In this paper, all specimens were made of normal-strength concrete. Accordingly, the scope of the work cannot extend to members made of high-strength concrete. Further study is needed to evaluate the ultimate strain and depth of the equivalent rectangular stress block suggested in the design code for RC beams. In addition, the technical review on a mechanical relationship between the RC beam specimens and the C-shaped specimens will be performed.

Acknowledgements

The authors would like to thank the Infra-Structures Assessment Research Center (ISARC) funded by Korea Ministry of Construction and Transportation (MOCT) for financial support. The fourth author wishes to thank the partial financial support from the KOSEF (Korea Science and Engineering Foundation), South Korea. These supports are deeply appreciated.

References

[1] Hillerborg A. Fracture mechanics concepts applied to moment capacity and rotational capacity of reinforced beams. In: Proceedings, international conference on fracture and damage mechanics of concrete and rock, Vienna; 1988; p. 233–40.
[2] Bazant ZP. Identification of strain-softening constitutive relation from uniaxial tests by series coupling model for localization. Cem Concr Res 1989;19:973–7.
[3] Cotterell B. Brittle fracture in compression. Int J Fract 1972;8(2): 195–208.
[4] Nemat-Nasser S, Obata M. A microcrack model of dilatancy in brittle material. J Appl Mech ASME 1988;55:24–35.
[5] Bazant ZP, Xiang Y. Size effect in compression fracture: splitting crack band propagation. J Eng Mech ASCE 1997;123(2):162–72.
[6] Gonnerman HF. Effect of size and shape of test specimen on compressive strength of concrete. Proceedings ASTM 1925;25: 237–50.
[7] Markeset G, Hillerborg A. Softening of concrete in compression localization and size effects. Cem Concr Res 1995;25(4):702–8.
[8] Jansen DC, Shah SP. Effect of length on compressive strain softening of concrete. J Eng Mech ASCE 1997;123(1):25–35.
[9] Fantilli AP, Ferretti D, Iori I, Vallini P. Mechanical model for failure of compressed concrete in reinforced concrete beams. J Struct Eng 2002;128(5):637–45.
[10] Bazant ZP, Kim JK. Size effect in shear failure of longitudinally reinforced concrete beams. ACI J Proc 1984;81(5):456–68.
[11] Bentz EC. Empirical modeling of reinforced concrete shear strength size effect for members without stirrups. ACI Struct J 2005;102(2): 232–41.
[12] Hognestad E, Hanson NW, McHenry D. Concrete stress distribution in ultimate strength design. J ACI Proc 1955;52:455–79. Also PCA Development Bulletin D6.
[13] Kaar PH, Hanson NW, Capell HT. Stress–strain characteristics of high-strength concrete. PCA Res Dev Bull RD051.01D 1977:1–10.
[14] ACI Committee 318-02, Building code requirements for structural concrete (ACI 318-02) and Commentary (ACI 318R-02). American Concrete Institute, Farmington Hills, MI, 2002; 443 pp.
[15] Kim JK, Yi ST, Yang EI. Size effect on flexural compressive strength of concrete specimens. ACI Struct J 2000;97(2):291–6.
[16] Kim JK, Yi ST, Kim JHJ. Effect of specimen sizes on flexural compressive strength of concrete. ACI Struct J 2001;98(3):416–24.
[17] Kim JHJ, Yi ST, Kim JK. Size effect of concrete members applied with flexural compressive stresses. Int J Fract 2004;126(1):79–102.
[18] Alca N, Alexander SDB, MacGregor JG. Effect of size on flexural behavior of high-strength concrete beams. ACI Struct J 1997;94(1): 59–67.
[19] Bazant ZP. Size Effect in blunt fracture; concrete, rock, metal. J Eng Mech ASCE 1984;110(4):518–35.
[20] Kim JK, Eo SH. Size effect in concrete specimens with dissimilar initial cracks. Mag Concr Res 1990;42(153):233–8.
[21] Bazant ZP. Fracture energy of heterogeneous material and similitude. In: SEM-RILEM International Conference on Fracture of Concrete and Rock; 1987. p. 390–02.
[22] Bazant ZP. Size effect in tensile and compressive quasibrittle failures. JCI International Workshop on Size Effect in Concrete Structures; 1993. p. 141–60.

[23] Kim JK, Yi ST, Park CK, Eo SH. Size effect on compressive strength of plain and spirally reinforced concrete cylinders. ACI Struct J 1999;96(1):88–94.
[24] Yi ST, Kim JHJ, Kim JK. Effect of specimen sizes on ACI rectangular stress block for concrete flexural members. ACI Struct J 2002;99(5):701–8.
[25] Yi ST, Yang EI, Choi JC. Effect of specimen sizes, specimen shapes, and placement directions on compressive strength of concrete. Nucl Eng Des 2006;236(2):115–27.
[26] Benjamin JR, Cornell CA. Probability, statistics, and decision for civil engineers. New York: McGraw-Hill; 1970. Section 4.3.
[27] IMSL, Library, Edition 8, IMSL, Inc.
[28] Corley GW. Rotational capacity of reinforced concrete beams. Proceedings ASCE 1966;92(ST5):121–46.
[29] Hubert R. Research towards a general flexural theory for structural concrete. J ACI Proc 1960;57(1):1–28.
[30] Nedderman H. Flexural stress distribution in very high strength concrete. Masters Degree Thesis. Department of Civil Engineering, University of Texas at Arlington; 1973.
[31] Nilson AH, Slate O. Structural properties of very high strength concrete. Second progress report. Department of Structural Engineering, Cornell University, Ithaca; 1979. 62 pp.